Long-range superexchange in $Cu_2A_2O_7$ (A = P, As, V) as a key element of the microscopic magnetic model

O. Janson,[1,*] A. A. Tsirlin,[1,†] J. Sichelschmidt,[1] Y. Skourski,[2] F. Weickert,[1,2,‡] and H. Rosner[1,§]

[1]*Max-Planck-Institut für Chemische Physik fester Stoffe, D-01187 Dresden, Germany*

[2]*Hochfeld-Magnetlabor Dresden, Helmholtz-Zentrum Dresden Rossendorf, D-01314 Dresden, Germany*

(Received 24 November 2010; revised manuscript received 7 February 2011; published 31 March 2011)

A microscopic magnetic model for α-$Cu_2P_2O_7$ is evaluated in a combined theoretical and experimental study. Despite a dominant intradimer coupling J_1, sizable interdimer couplings enforce long-range magnetic ordering at $T_N = 27$ K. The spin model for α-$Cu_2P_2O_7$ is compared to the models of the isostructural β-$Cu_2V_2O_7$ and α-$Cu_2As_2O_7$ systems. As a surprise, coupled dimers in α-$Cu_2P_2O_7$ and alternating chains in α-$Cu_2As_2O_7$ contrast with a honeycomb lattice in β-$Cu_2V_2O_7$. We find that the qualitative difference in the coupling regime of these isostructural compounds is governed by the nature of AO_4 side groups: d elements ($A = V$) hybridize with nearby O atoms forming a Cu-O-A-O-Cu superexchange path, while for p elements (A = P, As) the superexchange is realized via O-O edges of the tetrahedron. Implications for a broad range of systems are discussed.

DOI: 10.1103/PhysRevB.83.094435 PACS number(s): 71.20.Ps, 75.10.Jm, 75.30.Et, 75.50.Ee

I. INTRODUCTION

The search for new magnetic ground states (GSs) is an arduous challenge for condensed-matter physics. Since about two decades ago, the rapid development of computational techniques has spurred theoretical studies on various magnetic models. The recent observation of magnetic monopoles,[1] anticipated by a theoretical prediction,[2] is one of the most remarkable examples evidencing the excellent potential and reliability of sound theoretical studies.

Still, it is often tricky to find the way from a theoretical result to its experimental confirmation. In particular, the applicability of a theoretical model to a real material should be addressed. For magnetic systems, inelastic neutron-scattering (INS) experiments, which yield momentum-resolved excitation spectra for a wide range of energies and temperatures, are typically a method of choice. However, even the powerful neutron techniques are insecure against the ambiguous interpretation of experimental results. Thus, for instance, the analysis of INS data in Ref. 3 correctly disclosed the irrelevance of the two-leg Heisenberg spin-ladder model for the ambient-pressure modification of $(VO)_2P_2O_7$. At the same time, the experimental spectra exhibited a pronounced high-energy mode, and the authors of Ref. 3 interpreted it as a signature of a two-magnon bound state. Subsequent studies based on alternative techniques refuted this conjecture and revealed that the high-energy mode and the double-gap feature arise from two inequivalent alternating Heisenberg chains (AHCs) present in this system.[4] As another example, the frustrated Heisenberg chain $LiCu_2O_2$, had been proposed to imply two relevant antiferromagnetic (AF) exchange integrals J_1 and J_2, based on thermodynamical measurements and neutron-diffraction data,[5] while the combined nuclear magnetic resonance (NMR) and density-functional theory (DFT) study (Ref. 6) as well as the INS investigation (Ref. 7) revealed the ferromagnetic (FM) nature of J_1.

Recently, density-functional theory (DFT) calculations developed into an appealing alternative, complementary to experimental techniques. At present, the performance and reliability of DFT codes allow us to evaluate quantitative magnetic models even for complex materials, having only crystallographic information at hand. Moreover, DFT calculations are capable of even improving the structural input,[8] thus overcoming the problem of weakly scattering elements (for instance, H for x rays or V for neutrons) and the subsequently large error bars in the experimental atomic positions.

The inverse problem—to find a crystal structure for a specific spin lattice—is even more complex. Here, semiempirical Goodenough-Kanamori-Anderson (GKA) rules,[9] formulated about 60 years ago, still provide invaluable support. However, these rules are at best not universal. In particular, the GKA rules cannot be applied to long-range couplings that involve more than one ligand atom. The abundance of such couplings in real materials strongly motivates the development of further rules to account for these situations.

Semiempirical rules are especially helpful for a fine tuning of the material, because chemical substitutions usually alter exchange couplings or even the spin lattice. For example, the substitution of Br for Cl changes the singlet ground state of $(CuCl)LaNb_2O_7$ toward columnar AF ordering in the bromine compound.[10] The replacement of Zn by Mg in kapellasite $Cu_3Zn(OH)_6Cl_2$ leads to haydeeite $Cu_3Mg(OH)_6Cl_2$ with a reduced nearest-neighbor (NN) coupling and modified spin physics.[11]

In the present study, we perform a comparative investigation of the isostructural $Cu_2A_2O_7$ (A = P, As, V) compounds and consider an instructive example that is relevant for a family of systems with tetrahedral anions. The pentavalent nature of the A atoms ensures the magnetic $3d^9$ electronic configuration of Cu^{2+}. The thortveitite-type crystal structure of $Cu_2A_2O_7$ (Fig. 1, top) contains magnetic layers of Cu_2O_6 structural dimers (two edge-sharing CuO_4 plaquettes) coupled by nonmagnetic AO_4 tetrahedra. The neighboring layers are connected by two AO_4 tetrahedra forming A_2O_7 pyrophosphate, pyroarsenate, or pyrovanadate groups (Fig. 1, top right).

In this study, we disclose the underlying reason for a variety of magnetic behaviors— coupled spin dimers in α-$Cu_2P_2O_7$, alternating spin chains in α-$Cu_2As_2O_7$, and a honeycomb spin lattice in β-$Cu_2V_2O_7$—realized within the same basic crystal structure. Using DFT calculations, we evaluate five

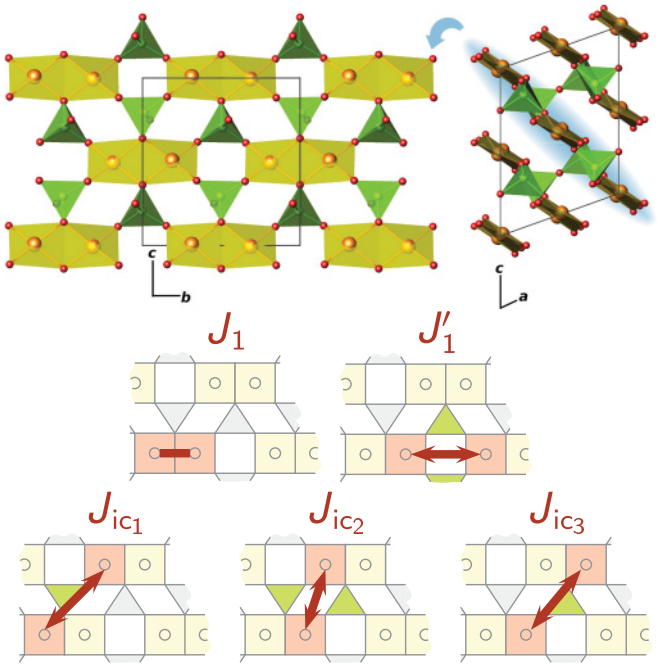

FIG. 1. (Color online) Crystal structure and exchange coupling paths in $Cu_2A_2O_7$ (A = P, As, V). Squares and triangles represent CuO_4 plaquettes and AO_4 tetrahedra, respectively.

relevant exchange couplings (Fig. 1, bottom). Surprisingly, these couplings are drastically affected by the electronic state of the side groups' central atom A, whether it is a p (P, As) or a d (V) element. Understanding the crucial role of nonmagnetic AO_4 groups is the key for directed chemical substitution, which may open the door for a tunable magnetism.

The magnetic properties of β-$Cu_2V_2O_7$ have been actively studied.[12] Very recently, we derived the actual spin model and identified an almost ideal spin-1/2 honeycomb lattice in this compound.[13] Considering the crystal structure of β-$Cu_2V_2O_7$, this magnetic model looks highly nontrivial. Puzzled by the driving force of such an unusual magnetic coupling regime, we prepared the isostructural system α-$Cu_2P_2O_7$ and investigated its magnetic behavior to allow for a comparative study.

$Cu_2P_2O_7$ has two polymorphic modifications. The low-temperature (α) and the high-temperature (β) phases reveal similar monoclinic crystal structures (Fig. 1), yet the β modification shows a twice smaller c lattice parameter and disordered arrangement of the oxygen atom shared by the two PO_4 tetrahedra of the pyrophosphate group.[14] In the following, we consider the α modification which is fully ordered and stable below 350 K. We would like to emphasize that this α modification is isostructural to the β modification of $Cu_2V_2O_7$. The magnetic behavior of α-$Cu_2P_2O_7$ was studied in the early 1970s. An AF ordering was found at 27 K, with tentative models of the magnetic structure established from neutron diffraction[15] and NMR.[16] However, no information on the microscopic magnetic model has been reported.

This paper is organized as follows. We introduce the methods used in our study in Sec. II. In Sec. III, we present our experimental as well as theoretical investigation of α-$Cu_2P_2O_7$. In Sec. IV, we compare the magnetic models of $Cu_2A_2O_7$ (A = P, As, V), and discuss the origin of their essentially different nature. Finally, in Sec. V, we summarize the results and give a short outlook.

II. METHODS

A single-phase powder sample of α-$Cu_2P_2O_7$ was prepared by a solid-state reaction of CuO and $NH_4H_2PO_4$. A stoichiometric mixture of the reagents was fired at 250 °C for 6 h in air to remove ammonia and water. The sample was further placed into a sealed quartz tube and heated at 800 °C for 12 h. The resulting light-gray powder was analyzed by x-ray-diffraction (Huber G670 Guinier camera, Cu$K_{\alpha 1}$ radiation, image plate detector, 3–100° angle range). A Rietveld refinement confirmed the formation of α-$Cu_2P_2O_7$ and did not show any traces of impurity phases (in particular, the admixture of β-$Cu_2P_2O_7$ can be ruled out). In contrast, a high-temperature annealing in air always produced a $Cu_3(PO_4)_2$ impurity.

Magnetic susceptibility (χ) was measured with a superconducting quantum interference device magnetometer (Quantum Design MPMS) in the temperature range 2–380 K in applied fields up to 5 T. High-field magnetization measurements (at $T = 1.4$ K) were performed at the Dresden High Magnetic Field Laboratory in pulsed fields up to 60 T. Details of the experimental procedure are described elsewhere.[17]

The electron spin resonance (ESR) spectra of a powder sample of α-$Cu_2P_2O_7$ were recorded at X-band frequencies (9.4 GHz) for temperatures 5–300 K. The spectra were fitted with a powder average of two Lorentzian lines corresponding to two (effective) components of the g tensor in axial symmetry: $g_\perp$ and $g_\parallel$.

DFT calculations were performed using the full-potential code FPLO9.00-31.[18] Within the local (spin) density approximation [L(S)DA], the exchange and correlation potential of Perdew and Wang has been used.[19]

For the LDA calculations, we chose a mesh of 1008 k points (207 in the irreducible wedge). Spin-polarized supercell LSDA $+U$ calculations were performed on 12, 18, and 32 k-point meshes.[20] All calculations were done for the experimental crystal structure from Ref. 14. To address the consistency of the structural data, we calculated forces and cross-checked the LDA results by using the generalized gradient approximation (GGA). Since the resulting forces do not exceed 1 eV/Å [the mean value is 0.7(3) eV/Å in both LDA and GGA], no further relaxation has been performed. The calculations were carefully checked for convergence.

Quantum Monte Carlo (QMC) simulations were performed on 24 × 24 finite lattices with periodic boundary conditions using the looper[21] and dirloop$_{sse}$ (directed loop in the stochastic series expansion representation)[22] algorithms from the ALPS package.[23]

III. MAGNETISM OF α-$Cu_2P_2O_7$

A. Magnetization and ESR measurements

The magnetic susceptibility $\chi(T)$ (Fig. 2, top) exhibits a broad maximum at $T_{max} = 54$ K indicative of low-dimensional behavior. The Curie-Weiss (CW) fit yields an AF Weiss temperature $\theta_{CW} = 61$ K and the effective moment of $1.89\mu_B$, slightly larger than the spin-only effective moment $\mu_{eff} = 2\sqrt{S(S+1)} \approx 1.73\mu_B$ for $S = 1/2$. The deviation from

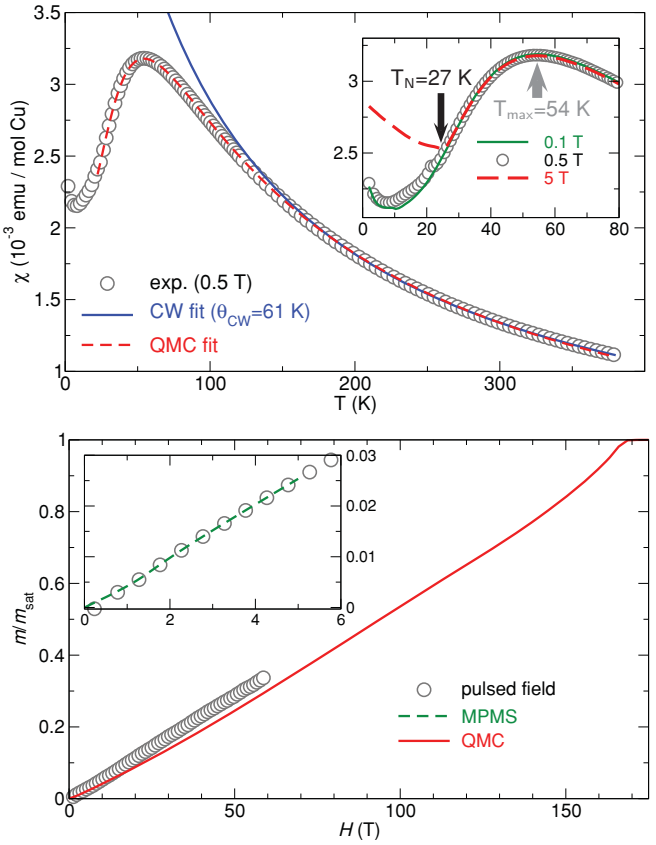

FIG. 2. (Color online) Top: magnetic susceptibility $\chi(T)$ of $Cu_2P_2O_7$ together with the Curie-Weiss (CW) and the quantum Monte Carlo (QMC) fits (see text). Inset: field dependence of $\chi(T)$. Bottom: high-field magnetization of $Cu_2P_2O_7$ with a QMC fit. Inset: scaling of the high-field magnetization curve with the MPMS data.

the CW fit below 140 K originates from the onset of AF correlations that lead to a long-range magnetic ordering at low temperatures.

The magnetic ordering transition is evidenced by a weak kink in the low-field $\chi(T)$ curves around $T_N \simeq 27$ K (circles and solid line in the upper inset of Fig. 2). The data measured at 5 T reveal a well-defined kink at the same temperature. The difference between the data collected in low and high fields below T_N should be related to the spin-flop transition around 1 T. The susceptibility upturn below 10 K is likely caused by a paramagnetic impurity contribution.

In order to estimate the g value and prove the AF ordering in $Cu_2P_2O_7$, we measured the electron spin resonance (ESR) of the Cu^{2+} spins as a local probe (Fig 3). The temperature dependencies of the integrated ESR absorption and $\chi(T)$ agree with each other (not shown). At elevated temperatures, both components of the g tensor ($g_\perp$ and $g_\parallel$) show typical values for the Cu^{2+} ion. An abrupt change in $g_\perp$ and $g_\parallel$ around $T_N = 27$ K indicates the onset of a strong internal magnetic field and thus confirms the magnetic ordering transition observed in the $\chi(T)$ data.

The magnetization $M(H)$ curve (Fig. 2, bottom) was scaled using the low-field (MPMS) data. It lacks any signatures of a spin gap and exhibits a linear behavior, incompatible with a simple dimer magnetism.

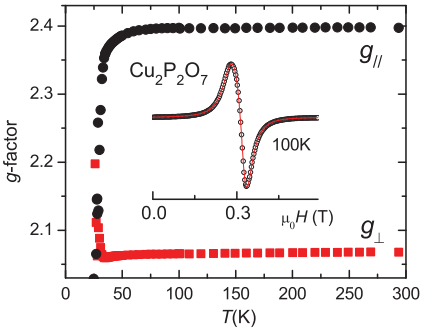

FIG. 3. (Color online) Temperature dependence of the g factor measured by the ESR of Cu^{2+}. The inset shows a typical derivative ESR spectrum (circles) fitted by two powder-averaged Lorentzian shapes (solid line).

B. DFT calculations

To evaluate the leading exchange couplings, we perform DFT band-structure calculations. For α-$Cu_2P_2O_7$, LDA yields a valence band with a width of 10 eV (Fig. 4, top), slightly larger than typical values for cuprates (7–8 eV).[11,24] The density of states (DOS) exhibits a peak at the Fermi level ϵ_F, evidencing a metallic GS, in contrast to the expected insulating behavior. This drawback of the LDA originates from the underestimation of correlation effects, intrinsic for the $3d^9$ electronic configuration of Cu^{2+}. To account for the correlation effects, we use two complementary approaches: (i) mapping the LDA bands onto a Hubbard model and (ii) adding correlations in a mean-field way within the band-structure scheme (LSDA + U calculations).

Despite the problem of correlations, LDA yields reliable information on the relevant orbitals and couplings. First, we project the DOS onto local orbitals of a CuO_4 plaquette. We find that the Cu states at ϵ_F have $3d_{x^2-y^2}$ character (Fig. 4, bottom right), resolving it as the magnetically active orbital.[25] Further on, the relevant couplings were identified

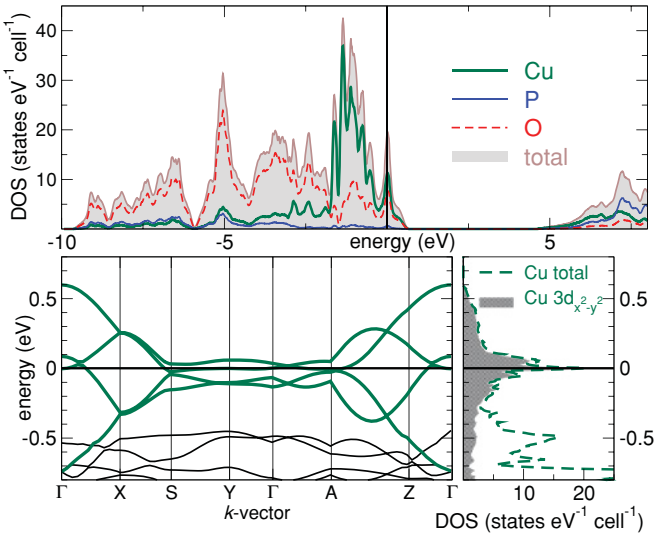

FIG. 4. (Color online) Density of states (top), band structure (bottom, left), and orbital-resolved density of states (bottom, right). The bands with $3d_{x^2-y^2}$ character are shown bold (green). The Fermi level is at zero energy.

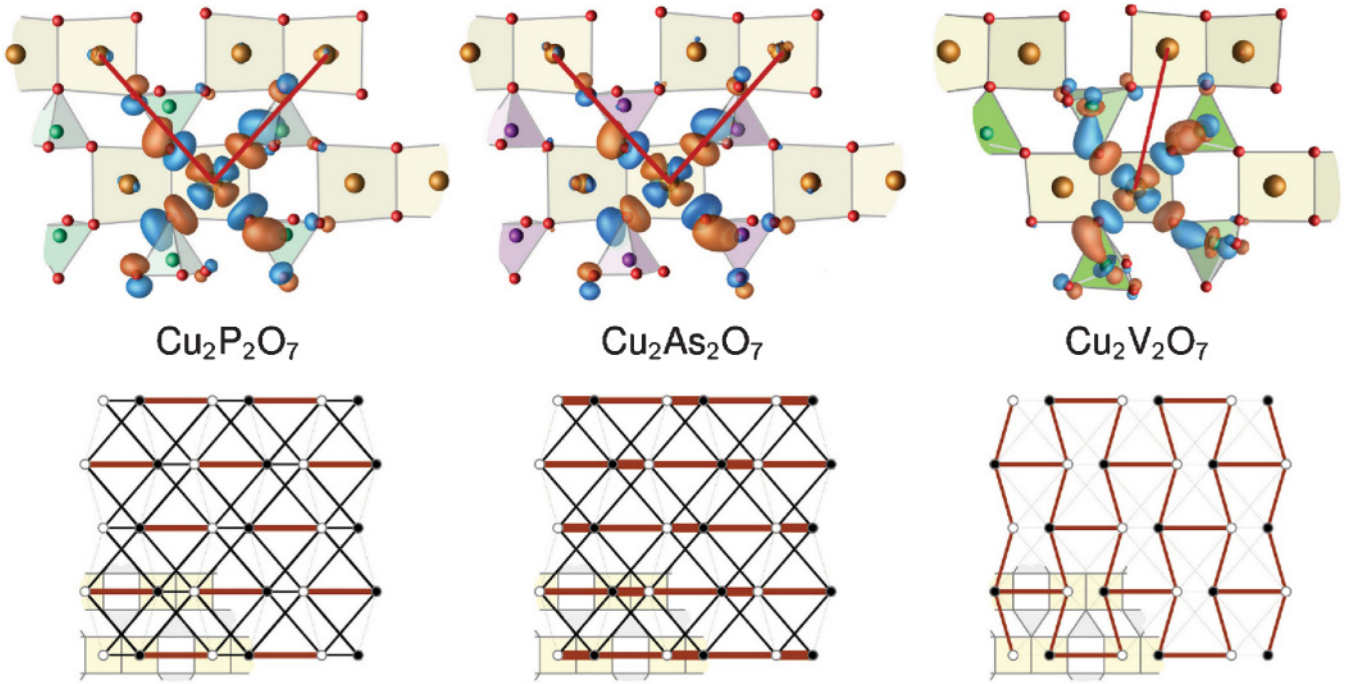

FIG. 5. (Color online) Top: Wannier functions for Cu $3d_{x^2-y^2}$ states with relevant interchain couplings (lines). Bottom: spin models for $Cu_2A_2O_7$ compounds. The thickness of a line reflects the magnitude of the respective coupling. Filled and empty circles represent up and down spins in the antiferromagnetically ordered state.

using Wannier functions (WFs) for the Cu $3d_{x^2-y^2}$ states.[26] The resulting fit is in excellent agreement with the LDA bands (Fig. 4, bottom left) and yields five relevant couplings. Two of them—the couplings within the structural dimer t_1 and between the structural dimers t_1' (Fig. 1, middle)—form alternating chains along the b axis. The chains are connected by two types of interchain couplings: t_{ic1} and t_{ic3} run through a single AO_4 tetrahedron, whereas t_{ic2} connects two Cu atoms with a double bridge of AO_4 tetrahedra (Fig. 1, bottom). Together with t_1 and t_1', these interchain couplings form the magnetic layers, parallel to (101), as shown in Fig. 1. The interlayer coupling of 30 meV is realized via pyrophosphate groups P_2O_7. Since it is substantially smaller than the leading terms, we neglect this coupling in the minimal model.

Here, we briefly remind the reader of the essential results for β-$Cu_2V_2O_7$ in Ref. 13: The WF analysis of the LDA bands revealed that t_1, t_1', and t_{ic2} couplings are relevant, while other terms are negligibly small (Table I). A mere comparison of t_i for α-$Cu_2P_2O_7$ with the respective values for β-$Cu_2V_2O_7$ readily yields several important results. First, the coupling t_1 within the structural dimer is essentially the same, while the inter-dimer coupling t_1' is slightly enhanced in α-$Cu_2P_2O_7$ compared to β-$Cu_2V_2O_7$. The similarity of the intrachain terms is in sharp contrast to the profound change in the interchain coupling regime: α-$Cu_2P_2O_7$ has sizable t_{ic1} and t_{ic3} with the negligibly small t_{ic2}, while for β-$Cu_2V_2O_7$ the situation is exactly the opposite. This results in clearly different band dispersions in α-$Cu_2P_2O_7$ (Fig. 4) and β-$Cu_2V_2O_7$ (Fig. 3 in Ref. 13).

To obtain the values of AF exchange integrals J_i^{AF}, we map the transfer integrals t_i from the WF-based analysis onto a Hubbard model. For the half filling and the strongly correlated limit $U_{eff} \gg t_i$, both well justified for undoped cuprates, magnetic excitations can be described by a Heisenberg model, while J_i^{AF} is expressed as $J_i^{AF} = 4t_i^2/U_{eff}$. This way, using a realistic value of 4.5 eV for the Coulomb repulsion U_{eff},[24] we obtain the AF part J_i^{AF} of the total exchange J_i (Table I).[27]

For the NN exchange coupling path X_1, the Cu-O-Cu angle is close to 90° (98.7° for β-$Cu_2V_2O_7$, 100.4° for α-$Cu_2P_2O_7$), suggesting a sizable ferromagnetic contribution according to the GKA rules.[9] Indeed, in many related systems this leads to a sizable reduction in the respective exchange J_i.[28] Moreover, in case the FM contribution exceeds J_i^{AF}, the resulting J_i exchange becomes FM.[29] Therefore to complete the spin model, it is necessary to calculate the values of total exchange integrals J_i, being the sum of the AF and FM contributions. We evaluate the numerical values by performing spin-polarized LSDA + U supercell calculations for various collinear spin arrangements and map the total energies onto a classical Heisenberg model. Following the conclusions of Ref. 13, we choose the around-mean-field double-counting-correction

TABLE I. Transfer (t_i, in meV) and exchange (J_i, in K) integrals for α-$Cu_2P_2O_7$ and β-$Cu_2V_2O_7$. J_i^{AF} (in K) are calculated as $4t_i^2/U_{eff}$ (see text).

Path	α-$Cu_2P_2O_7$			β-$Cu_2V_2O_7$(Ref. 13)		
	t_i	J_i^{AF}	J_i	t_i	J_i^{AF}	J_i
X_1	156	251	34	148	226	5
X_1'	103	109	102	−84	73	61
X_{ic_1}	83	71	46	18	3	
X_{ic_2}	−12	1		97	97	87
X_{ic_3}	79	64	41	−15	2	

(DCC) and $U_d = 6.5$ eV.[30] The resulting exchange integrals J_i are given in Table I.[31]

For α-$Cu_2P_2O_7$, a sizable FM contribution of $J_1^{\rm FM} \sim -230$ K considerably reduces the coupling within the structural dimer, as in β-$Cu_2V_2O_7$. Again similar to β-$Cu_2V_2O_7$, the interdimer coupling J_1' has a tiny FM contribution only.[32] However, in α-$Cu_2P_2O_7$, J_1' is clearly dominant and seemingly favors a dimerlike magnetism with magnetic dimers located between the structural dimers Cu_2O_6. All interchain couplings are long range, and their FM contributions are likely to be small. Indeed, we find $J_{\rm ic_1}^{\rm FM} \approx J_{\rm ic_3}^{\rm FM} \sim -20$ K consistent with $J_{\rm ic_2}^{\rm FM} = -10$ K found for β-$Cu_2V_2O_7$.[13] Noteworthy for the closely related system $Cu_2(PO_3)_2(CH_2)$, similar values have been reported.[33] To summarize, for α-$Cu_2P_2O_7$ we arrive at the two-dimensional (2D) magnetic model with a strongly dominant J_1' and three additional relevant couplings, rather different from the 2D honeycomb lattice system β-$Cu_2V_2O_7$ as well as from the structurally related but essentially one-dimensional (gapped $J_1 - J_1'$ chains) $(VO)_2P_2O_7$ in its high-pressure modification.[34]

Despite the 2D nature of the spin models, the magnetic GSs of α-$Cu_2P_2O_7$ and β-$Cu_2V_2O_7$ are AF ordered.[15,35] Since thermal fluctuations in purely 2D Heisenberg systems exclude long-range magnetic order at finite temperatures,[36] the coupling perpendicular to the magnetic layers should be addressed. In β-$Cu_2V_2O_7$, effective superexchange paths along the $[V_2O_7]$ pyrovanadate groups give rise to a sizable long-range interlayer exchange $J_\perp = 17$ K.[13] In contrast, the interlayer couplings in α-$Cu_2P_2O_7$ are much weaker and short-range: Although the transfer integral associated with the shortest interlayer coupling (Cu–Cu distance 3.33 Å) amounts to $t_{\perp 1} = 31$ meV, the LSDA $+ U$ calculations reveal a sizable FM contribution that largely reduces this coupling to about $J_{\perp 1} = 1$ K. The next largest ($t_{\perp 2} = 18$ meV) interlayer coupling corresponds to the Cu-Cu distance of 3.88 Å, and gives rise to a magnetic exchange of 3–4 K.

Using the interlayer couplings resulting from the DFT calculations, we find one more difference between α-$Cu_2P_2O_7$ and β-$Cu_2V_2O_7$. In β-$Cu_2V_2O_7$, the magnetic structure should break the C centering of the unit cell,[13] whereas the long-range order in α-$Cu_2P_2O_7$ inherits the full crystallographic symmetry (the $C2/c$ space group). The distinct patterns of the magnetic ordering should be resolvable by high-precision neutron diffraction and could be an ultimate experimental test of our predictions. The lack of magnetic reflections in the available neutron data for α-$Cu_2P_2O_7$ (Ref. 15) indicates that the magnetic order does not break any crystallographic symmetry, nor leads to the formation of a magnetic superstructure, in accord with our microscopic model.

C. Model simulations

To justify the proposed spin model for α-$Cu_2P_2O_7$, we perform QMC simulations of the magnetic susceptibility and the high-field magnetization data. First, to fit the calculated susceptibility to the experiment (Fig. 2), we keep the ratios $J_1/J_1' = 0.33$, $J_{\rm ic_1}/J_1' = 0.45$, and $J_{\rm ic_3}/J_1' = 0.40$ from the DFT calculations (Table I), and vary the absolute values of J_1' and g.[37] This way, we obtain an excellent agreement with the experimental curve down to the ordering temperature $T_N = 27$ K (Fig. 2). The resulting $J_1' = 79$ K and $g = 2.21$ are in reasonable agreement with $J_1' = 102$ K from the LSDA $+ U$ calculations and the powder-averaged $g = (2g_\perp + g_\parallel)/3 = 2.18$ from ESR.

The simulated magnetization curve (Fig. 2, bottom) is scaled adopting $J_1' = 79$ K and $g = 2.21$ from the fit to the magnetic susceptibility.[38] The overall agreement with the experiment is rather good, while the discrepancy likely arises from the imperfectness of the scaling of the experimental high-field curve. In particular, the scaling is done based on a very narrow low-field region (up to 5 T, see the inset of Fig. 2), which might be affected by paramagnetic impurities.

IV. DISCUSSION

The spin models of α-$Cu_2P_2O_7$ and β-$Cu_2V_2O_7$ are essentially different: whereas α-$Cu_2P_2O_7$ is a system of coupled dimers, β-$Cu_2V_2O_7$ is an almost isotropic honeycomb lattice. In β-$Cu_2V_2O_7$, a strong FM contribution practically "switches off" the coupling within the structural dimers (J_1), leaving only the couplings between the structural dimers (J_1') and between the chains ($J_{\rm ic_2}$) relevant (Fig. 5, bottom right).[13] On the contrary, α-$Cu_2P_2O_7$ has a dominant J_1', smaller $J_{\rm ic_1}$ and $J_{\rm ic_3}$ (see Fig. 1 for the notation of the exchange couplings), as well as even smaller J_1 (Fig. 5, bottom left). The striking dissimilarity of the two models leads to a question, whence this difference originates.

To address this puzzling issue, we consider another $Cu_2A_2O_7$ system, α-$Cu_2As_2O_7$, and briefly report the key results of our DFT calculations. In particular, the WF analysis yields values of transfer integrals t_i similar to those of α-$Cu_2P_2O_7$. The total exchange integrals, derived from the results of LSDA $+ U$ calculations, are somewhat larger than the respective exchange couplings for α-$Cu_2P_2O_7$. However, the only pronounced difference between the magnetic models of α-$Cu_2P_2O_7$ and α-$Cu_2As_2O_7$ is the strong enhancement of the NN coupling J_1 in the latter system (Fig. 5, bottom middle). A detailed experimental and theoretical analysis of the magnetic properties of α-$Cu_2As_2O_7$ is presently underway.[39]

So far, we find the resemblance of the spin models of α-$Cu_2P_2O_7$ and α-$Cu_2As_2O_7$, whereas β-$Cu_2V_2O_7$ is remarkably different. The common feature of these compounds is the sizable AF coupling J_1' forming spin dimers. The interdimer couplings are, however, different. In α-$Cu_2P_2O_7$ and α-$Cu_2As_2O_7$, the interdimer couplings run through a single AO_4 tetrahedron ($J_{\rm ic_1}$ and $J_{\rm ic_3}$), while in β-$Cu_2V_2O_7$ only the coupling via a double bridge of AO_4 tetrahedra is relevant.

As we know from the analysis of the band structure, the magnetism of $Cu_2A_2O_7$ systems originates from the half filled Cu $3d_{x^2-y^2}$ orbitals. Above, we used the WF for this magnetically active orbital to obtain the relevant couplings (Sec. III B). However, the fact that WF are defined in real space makes them capable of tracing the superexchange path.[40] In Fig. 5, we plot the WF for the three systems.

As expected from the similarity of the band structures, the WFs for α-$Cu_2P_2O_7$ and α-$Cu_2As_2O_7$ are very similar.[41] Note (i) the absence of P or As contributions and (ii) the antibonding combination formed by WF contributions along Cu-O-O-Cu paths, favoring $t_{\rm ic1}$ and $t_{\rm ic3}$ couplings. In contrast, the WF of β-$Cu_2V_2O_7$ shows sizable weight on V atoms, exhibiting a shape

reminiscent of the $d_{3z^2-r^2}$ orbital. These V states hybridize with the nearby O orbitals thus forming an effective superexchange path Cu-O-V-O-Cu. The V-O hybridization drastically alters the interchain coupling regime, now favoring J_{ic_2} exchange via a double bridge of VO_4 tetrahedra.

As evidenced by numerous examples, the replacement of anionic groups can stabilize different crystal structures. Thus the replacement of Se by a larger Te atom transforms the chain-like structure of $CuSe_2O_5$ into complex 2D layers of $CuTe_2O_5$. Not surprisingly, this structural change drastically affects the magnetism: While $CuSe_2O_5$ shows Heisenberg chain physics and AF order,[13] $CuTe_2O_5$ has a dimerized magnetic GS.[42] However, it is commonly believed that the replacement of a nonmagnetic part, *not accompanied* by structural changes, should have a minor impact on magnetism. Our study shows that this conjecture is not universal. In particular, the electronic configuration of the nonmagnetic group should be addressed. Thus the d states of V in β-$Cu_2V_2O_7$ are strongly mixed with the p states of oxygen (see Fig. 2 in Ref. 13), allowing for a strong superexchange along the largely covalent V-O bonds. On the contrary, p cations like P or As donate electrons to the neighboring O atoms, giving rise to more ionic P(As)-O bonds. In this case, electron hopping between P(As) and O atoms becomes energetically unfavorable thus confining the superexchange to the Cu-O-O-Cu path.

Regarding the superexchange in transition-metal phosphates, the lack of the P contribution to the magnetic orbital and the crucial role of M-O-O-M pathways has been recently established for the related spin-$\frac{1}{2}$ V^{+4} compounds. A systematic study of model structures with different bond distances and angles puts forward the M-O and O-O distances as key structural parameters that determine the coupling strength.[43,44] Another relevant feature is the number of bridging tetrahedral groups. Given similar bond distances, a double bridge makes two superexchange pathways, which are more efficient than a single bridge.[45] This trend holds for α-$Cu_2P_2O_7$, where the double-bridge coupling J_1' is stronger than the single-bridge exchanges J_{ic1} and J_{ic3} (Table I). An important difference between copper and vanadium phosphates is the stronger metal-oxygen hybridization in the former case. The hybridization, amplified by the σ-type bonding between Cu $d_{x^2-y^2}$ and oxygen p orbitals, leads to a non-negligible contribution of second-neighbor oxygen atoms to WF (see Fig. 5). In $BiCu_2PO_6$, such "tails" of WF are responsible for the pronounced difference between the seemingly equivalent long-range couplings.[28] A comparative study of Cu^{+2} and V^{+4} compounds could facilitate further development of empirical rules for the superexchange. The $Cu_2A_2O_7$ structures are especially apposite for this purpose due to their similarity to $(VO)_2P_2O_7$, CsV_2O_5, $VOSeO_3$, and other V^{+4} oxides.

Generalizing the results, our study evidences that for the tetrahedral nonmagnetic AO_4 groups with the central p atom the magnetic superexchange is realized via an O-O edge of the tetrahedron. In contrast, a tetrahedrally coordinated 3d element gives rise to a strong hybridization with O 2p orbitals and a concomitant change in the superexchange path. This finding constitutes an empirical rule to estimate the relevant long-range couplings in a wide range of low-dimensional systems containing nonmagnetic tetrahedral side groups.

V. SUMMARY AND OUTLOOK

To summarize, we presented a comprehensive experimental (magnetic susceptibility, ESR, and high-field magnetization) and theoretical (full-potential DFT calculations) investigation of the magnetism of α-$Cu_2P_2O_7$. This material implies a two-dimensional magnetic model of strongly coupled magnetic dimers, which interestingly does not lead to a singlet ground state: Sizable interdimer couplings enforce the antiferromagnetic ordering at 27 K.

The coupled dimer model of α-$Cu_2P_2O_7$ is essentially different from the honeycomb lattice model, realized in the isostructural system β-$Cu_2V_2O_7$. Based on a comparison between α-$Cu_2P_2O_7$, α-$Cu_2As_2O_7$, and β-$Cu_2V_2O_7$, we unravel the crucial importance of the nonmagnetic AO_4 side groups for the magnetism of $Cu_2A_2O_7$ (A = P, As, V) systems: Whereas a d atom (V) strongly hybridizes with the ligand O orbitals, the p states (P, As) do not contribute to the superexchange path. Within the structure of $Cu_2A_2O_7$ compounds, this leads to a drastic change in the topology of the interchain couplings. The forthcoming experimental study of α-$Cu_2As_2O_7$ should provide a deeper insight into the magnetism of this system and challenge our findings.[39] Our results can be applied to tune the magnetism of systems comprising a similar structural motive, for instance, $Cu_2(PO_3)_2(CH_2)$ (Ref. 33) or $(VO)_2P_2O_7$ (Ref. 34).

Our study emphasizes the danger to use isostructural compounds as reference or analog. Such comparisons, unless based on a precise knowledge of the underlying electronic structure, are at best not justified and can be completely misleading. Instead, they are amenable to a careful verification. The latter can be reliably performed by electronic structure calculations that provide a microscopic insight into the electronic and magnetic properties even of complex compounds.

ACKNOWLEDGMENTS

We are grateful to Yurii Prots and Horst Borrmann for x-ray-diffraction measurements, and to Walter Schnelle for fruitful discussions and valuable comments. Part of this work has been supported by EuroMagNET II under EU Contract No. 228043. A.T. acknowledges funding from Alexander von Humboldt Foundation.

*janson@cpfs.mpg.de
†altsirlin@gmail.com
‡Present address: Los Alamos National Laboratory, Los Alamos, New Mexico 87545, USA.
§rosner@cpfs.mpg.de

[1] S. T. Bramwell, S. R. Giblin, S. Calder, R. Aldus, D. Prabhakaran, and T. Fennell, Nature (London) **461**, 956 (2009).
[2] C. Castelnovo, R. Moessner, and S. L. Sondhi, Nature (London) **451**, 42 (2008).

[3]A. W. Garrett, S. E. Nagler, D. A. Tennant, B. C. Sales, and T. Barnes, Phys. Rev. Lett. **79**, 745 (1997).
[4]T. Yamauchi, Y. Narumi, J. Kikuchi, Y. Ueda, K. Tatani, T. C. Kobayashi, K. Kindo, and K. Motoya, Phys. Rev. Lett. **83**, 3729 (1999).
[5]T. Masuda, A. Zheludev, A. Bush, M. Markina, and A. Vasiliev, Phys. Rev. Lett. **92**, 177201 (2004); S.-L. Drechsler, J. Málek, J. Richter, A. S. Moskvin, A. A. Gippius, and H. Rosner, *ibid.* **94**, 039705 (2005); T. Masuda, A. Zheludev, A. Bush, M. Markina, and A. Vasiliev, *ibid.* **94**, 039706 (2005).
[6]A. A. Gippius, E. N. Morozova, A. S. Moskvin, A. V. Zalessky, A. A. Bush, M. Baenitz, H. Rosner, and S.-L. Drechsler, Phys. Rev. B **70**, 020406 (2004).
[7]T. Masuda, A. Zheludev, B. Roessli, A. Bush, M. Markina, and A. Vasiliev, Phys. Rev. B **72**, 014405 (2005).
[8]A. A. Tsirlin and H. Rosner, Phys. Rev. B **79**, 214416 (2009); C.-Y. Ren and C. Cheng, *ibid.* **82**, 024404 (2010); A. A. Tsirlin, A. M. Abakumov, G. Van Tendeloo, and H. Rosner, *ibid.* **82**, 054107 (2010); C. Tassel, J. Kang, C. Lee, O. Hernandez, Y. Qiu, W. Paulus, E. Collet, B. Lake, T. Guidi, M.-H. Whangbo, C. Ritter, H. Kageyama, and S.-H. Lee, Phys. Rev. Lett. **105**, 167205 (2010).
[9]J. B. Goodenough, Phys. Rev. **100**, 564 (1955); J. Kanamori, J. Phys. Chem. Solids **10**, 87 (1959); P. W. Anderson, Phys. Rev. **79**, 350 (1950).
[10]Y. Tsujimoto, A. Kitada, H. Kageyama, M. Nishi, Y. Narumi, K. Kindo, Y. Kiuchi, Y. Ueda, Y. J. Uemura, Y. Ajiro, and K. Yoshimura, J. Phys. Soc. Jpn. **79**, 014709 (2010).
[11]O. Janson, J. Richter, and H. Rosner, Phys. Rev. Lett. **101**, 106403 (2008).
[12]M. Yashima and R. O. Suzuki, Phys. Rev. B **79**, 125201 (2009).
[13]A. A. Tsirlin, O. Janson, and H. Rosner, Phys. Rev. B **82**, 144416 (2010).
[14]K. Pogorzelec-Glaser, A. Pietraszko, B. Hilczer, and M. Połomska, Phase Transit. **79**, 535 (2006).
[15]J. A. R. Stiles and C. V. Stager, Can. J. Phys. **50**, 3079 (1972).
[16]J. A. R. Stiles and C. V. Stager, Can. J. Phys. **51**, 87 (1973).
[17]A. A. Tsirlin, B. Schmidt, Y. Skourski, R. Nath, C. Geibel, and H. Rosner, Phys. Rev. B **80**, 132407 (2009).
[18]K. Koepernik and H. Eschrig, Phys. Rev. B **59**, 1743 (1999).
[19]J. P. Perdew and Y. Wang, Phys. Rev. B **45**, 13244 (1992).
[20]Supercells contain a doubled number of atoms compared to the crystallographic unit cell. In addition, spin-polarized calculations require a quadrupled matrix compared to LDA calculations. This leads to a substantial increase in the computation time. Therefore only less dense k meshes can be used.
[21]S. Todo and K. Kato, Phys. Rev. Lett. **87**, 047203 (2001).
[22]F. Alet, S. Wessel, and M. Troyer, Phys. Rev. E **71**, 036706 (2005), and references therein.
[23]A. Albuquerque, F. Alet, P. Corboz, P. Dayal, A. Feiguin, S. Fuchs, L. Gamper, E. Gull, S. Gürtler, A. Honecker, R. Igarashi, M. Körner, A. Kozhevnikov, A. Läuchli, S. R. Manmana, M. Matsumoto, I. P. McCulloch, F. Michel, R. M. Noack, G. Pawlowski, L. Pollet, T. Pruschke, U. Schollwöck, S. Todo, S. Trebst, M. Troyer, P. Werner, and S. Wessel, J. Magn. Magn. Mater. **310**, 1187 (2007).
[24]O. Janson, R. O. Kuzian, S.-L. Drechsler, and H. Rosner, Phys. Rev. B **76**, 115119 (2007).
[25]Despite the geometrical distortion of CuO_4 units, resulting in a small hybridization of Cu $3d_{x^2-y^2}$ states with other Cu states (Fig. 4, bottom left), this hybridization is far too small to affect the orbital ground state.
[26]H. Eschrig and K. Koepernik, Phys. Rev. B **80**, 104503 (2009).
[27]Exchange integrals J_i^{AF} sharpen the trends inferred from the analysis of t_i's: $J_{\mathrm{ic}_1}^{\mathrm{AF}}$ and $J_{\mathrm{ic}_3}^{\mathrm{AF}}$ are relevant for α-$Cu_2P_2O_7$, while $J_{\mathrm{ic}_2}^{\mathrm{AF}}$ is relevant for β-$Cu_2V_2O_7$.
[28]A. A. Tsirlin, I. Rousochatzakis, D. Kasinathan, O. Janson, R. Nath, F. Weickert, C. Geibel, A. M. Läuchli, and H. Rosner, Phys. Rev. B **82**, 144426 (2010).
[29]O. Janson, A. A. Tsirlin, M. Schmitt, and H. Rosner, Phys. Rev. B **82**, 014424 (2010).
[30]The access to all relevant couplings is ensured by considering three different supercells.
[31]LSDA + U calculations correctly reproduce the insulating ground state in the physically relevant range of $U_d = 5.5 - 7.5$eV, yielding the band gap of about 3.3(6)eV for $Cu_2P_2O_7$ and 2.9(3)eV for $Cu_2As_2O_7$.
[32]M. D. Johannes, J. Richter, S.-L. Drechsler, and H. Rosner, Phys. Rev. B **74**, 174435 (2006).
[33]M. Schmitt, A. A. Gippius, K. S. Okhotnikov, W. Schnelle, K. Koch, O. Janson, W. Liu, Y.-H. Huang, Y. Skourski, F. Weickert, M. Baenitz, and H. Rosner, Phys. Rev. B **81**, 104416 (2010).
[34]D. C. Johnston, T. Saito, M. Azuma, M. Takano, T. Yamauchi, and Y. Ueda, Phys. Rev. B **64**, 134403 (2001).
[35]Z. He and Y. Ueda, Phys. Rev. B **77**, 052402 (2008).
[36]N. D. Mermin and H. Wagner, Phys. Rev. Lett. **17**, 1133 (1966).
[37]The details of the fitting procedure are extensively discussed in Ref. 29.
[38]The uncertainty of such scaling can reach 30–40%, which largely exceeds typical uncertainties of $\chi(T)$ measurements. Therefore the fitting of the magnetic exchange couplings is done using $\chi(T)$ data only.
[39]Y. Arango, E. Vavilova, V. Kataev, R. Klingeler, A. A. Tsirlin, O. Janson, S.-L. Drechsler, H. Rosner, and B. Büchner (unpublished).
[40]O. Janson, W. Schnelle, M. Schmidt, Yu. Prots, S.-L. Drechsler, S. K. Filatov, and H. Rosner, New J. Phys. **11**, 113034 (2009).
[41]The only visible difference is the larger weight of the Wannier function on the neighboring copper atom (corresponding to t_1 coupling) in the case of α-$Cu_2As_2O_7$, in line with the enhanced value J_1 in α-$Cu_2As_2O_7$ compared to α-$Cu_2P_2O_7$.
[42]J. Deisenhofer, R. M. Eremina, A. Pimenov, T. Gavrilova, H. Berger, M. Johnsson, P. Lemmens, H.-A. Krug von Nidda, A. Loidl, K.-S. Lee, and M.-H. Whangbo, Phys. Rev. B **74**, 174421 (2006).
[43]A. A. Tsirlin and H. Rosner, Phys. Rev. B **79**, 214417 (2009).
[44]A. A. Tsirlin, R. Nath, A. M. Abakumov, R. V. Shpanchenko, C. Geibel, and H. Rosner, Phys. Rev. B **81**, 174424 (2010).
[45]M. Roca, P. Amorós, J. Cano, M. Dolores Marcos, J. Alamo, A. Beltrán-Porter, and D. Beltrán-Porter, Inorg. Chem. **37**, 3167 (1998).